Available on CMS information server **CMS NOTE 1997/108**

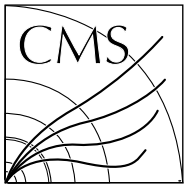

The Compact Muon Solenoid Experiment

CMS Note

Mailing address: CMS CERN, CH-1211 GENEVA 23, Switzerland

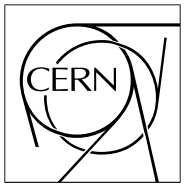

June 16, 1997

Test beam results on single-sided irradiated silicon microstrip detectors

P. Azzi, N. Bacchetta, D. Bisello, G. Busetto, A. Castro, M. Loreti
G. Martignon, D. Pantano, I. Stavitski

CMS Tracker Collaboration
Università di Padova and I.N.F.N. Sezione di Padova

Abstract

We present test beam results on irradiated AC-coupled, poly biased, single sided (p^+ on n-bulk) silicon microstrip detectors. Detectors were fabricated at SINTEF (Oslo, Norway); they have 128 strips, a strip pitch of 50 μm, strip width 12.5 μm and a length of 5.5 cm. Neutron doses were 1×10^{13} and 3.6×10^{13} n/cm^2 and we estimated the γ dose from the neutron irradiation facility background to be enough to induce full saturation in the oxide trapped charge value. Anti-annealing processes were accelerated via heat treatment to ensure stable operational depletion and leakage current values during data taking.

Three modules were constructed, one for each value of neutron dose, and one with non irradiated detectors using two crystals bonded together to form a 11 cm long readout unit. Data was taken at room temperature using the CERN 120 GeV π^+ beam (at X7) for different beam angle of incidence (0°, 20°, 35°) as a function of $V_{\rm bias}$ up to values of 330 V. For the most irradiated module we also took data with 100 μm readout pitch (alternate readout scheme) at 330 V.

No appreciable performance losses were observed for these levels of radiation damage as long as the detectors could be operated at suitably high bias voltages.

1 Introduction

When exposed to high radiation doses such as those found in the tracking volume of the LHC experiments, silicon detectors undergo type inversion, they reach high depletion voltages and high values of leakage currents and they will quickly saturate their oxide trapped charge value. All these effects change the properties of the detectors and careful beam studies should be carried out to ensure their satisfactory application in such high radiation dose environments.

The aim of this work is to assess the feasibility of using single sided (p^+ on n-type substrate) detectors at doses beyond type inversion, the main point being finding a reasonable bias voltage at which to recover the original performances, if at all possible.

2 Irradiation and modules preparation

The detectors we used are single sided silicon microstrip detectors fabricated at SINTEF and developed within the RD20 collaboration [1]. They are very simple device with a single guard ring and without any particular rad-hard option (such as multi guard rings, surrounding n^+ implant or deep implantation procedures). The main characteristics of these detectors before irradiation are summarised in table 1.

strip pitch	50 µm
implant width	12.5 µm
number of strips	128
strip length	5.5 cm
detector thickness	300 µm
V_{depl}	40 V
I_{leak} (per strip)	40 nA
$C_{\mathrm{interstrip}}$	4 pF
C_{coupl}	120 pF
R_{bias}	2.5 MΩ

Table 1: Detectors characteristics

Four detectors were irradiated (room temperature, bias off) at the CERN PS-ACOL facility [2] using 1 MeV neutrons, two at the dose of 1×10^{13} n/cm^2 and two at 3.6×10^{13} n/cm^2. Doses were chosen such that both pairs would undergo type inversion maintaining a reasonable value of depletion voltage. We verified that our detectors could bear a bias voltage of at least 350 V before irradiation, therefore allowing for performance studies at large values of overdepletion.

A few days after the irradiation (crystals were always kept at room temperature) the electrical characteristics of the detectors were measured at the probe station.

Measurement results and predicted values[1)] are in table 2.

Notice that the interstrip capacitance value is the same for both doses implying that the saturation value for the charge trapped in the oxide was reached already at the lowest dose.

After these measurements the four crystals were heated (12 hours at 80°C) in order to accelerate,

[1)] Predicted values of V_{depl} after irradiation and after heating are calculated with this ([3],[4])

	Dose (n/cm^2)	
	1×10^{13}	3.6×10^{13}
$V_{\rm depl}$ (measured)	17 V	30 V
$V_{\rm depl}$ (predicted)	10 V	36 V
$I_{\rm leak}$ (per strip)	270 nA	605 nA
$I_{\rm leak}$ (predicted)	288 nA	931 nA
$C_{\rm interstrip}$	6 pF	6 pF
$C_{\rm coupl}$	110 pF	110 pF
$R_{\rm bias}$	1.5 MΩ	1.3 MΩ

Table 2: Electrical characteristics after irradiation.

up to completion, the annealing/antiannealing processes, reaching stable conditions (in terms of both leakage current and depletion voltage) for all the detectors. With this choice (the heat treatment and the room temperature operation) we worsened the operational conditions of the detectors and, to some extent (for instance the depletion voltage), this condition is similar to higher irradiation values (the heat treatment for instance brings the detectors irradiated at 3.6×10^{13} to a depletion voltage value that would have been reached at a dose of $\geq 1 \times 10^{14}$ n/cm^2 and $T < 5^{\circ}$C).

Measurements after the heating treatment are summarised in table 3 and are in agreement with expectations (see [3] and [4]). These values are very stable with time, being the same even after several months.

	Dose (n/cm^2)	
	1×10^{13}	3.6×10^{13}
$V_{\rm depl}$ (measured)	70 V	140 V
$V_{\rm depl}$ (predicted)	43 V	156 V
$I_{\rm leak}$ (per strip)	125 nA	270 nA
$I_{\rm leak}$ (predicted)	135 nA	302 nA
$C_{\rm interstrip}$	6 pF	6 pF

Table 3: Electrical characteristics after irradiation and heating treatment.

Three modules were assembled using two crystals bonded together to form 11 cm long strips,

---

parametrization of $N_{\rm eff}$ as a function of received dose Φ and time:

$$N_{\rm eff}(\Phi,t,T) = N_{\rm eff}(0) - N_D(0)\cdot(1-e^{-c\Phi}) - g_c\Phi - g_y\Phi\cdot R(t,T)$$
$$R(t,T) = 1 - e^{t\cdot\Phi\cdot 24\cdot exp(-\frac{1.5\times 10^{-4}}{T})}$$

with these constants ([3]): $c \approx 3\cdot 10^{-13}$ cm^2; $g_c \approx 0.015$ cm^{-1}; $g_y \approx 0.05$ cm^{-1}; and $N_{\rm eff}(0) \approx N_D(0) \approx 6\times 10^{11}$ cm^3.
The parametrization for $I_{\rm leak}$ is [3]:

$$I(\Phi) = I_0 + \alpha\cdot\Phi\cdot Vol \qquad \alpha \simeq 3.0\cdot 10^{-17}{\rm A/cm} \qquad I(T) \simeq T^2\cdot e^{-\frac{E_g}{2kT}}$$

one for each of the two doses (module *pd2* using 1×10^{13} crystals and module *pd3* using 3.6×10^{13} crystals) and one with non irradiated detectors (module *pd1*).

Each pair of crystals is glued on a G10 frame and mounted on the standard frame system used by the CMS group for test beam studies [5]. Each strip was bonded via a pitch adapter to a 128-PreMux readout chip set to have a shaping time of 45 ns and readout speed of about 0.5 MHz. Details on the chip performance can be found in [6].

Noise measurements[2)] were taken during the test beam as a function of V_{bias} (fig.1) and in Padova with a different DAQ. The noise behaviour strictly follows the increased capacitance value with dose and the slight decrease of the latter with applied bias voltage.

We also compared the noise of *pd3* with two different readout pitches (fig.2) as a function of leakage current. The leakage current was artificially increased via heating in order to compare noise performances for the two readout schemes with theoretical calculations. As expected the 100 µm readout scheme has a slightly lower noise value (due to a lower interstrip capacitance). For both readout schemes the leakage current has to reach a value of about 1 µA/strip before having a significant role in the measured total noise[3)]. Using the same formulas described in [3] we expect to reach about 1 µA/strip after an accumulated dose of $\simeq 2 \times 10^{14}$ p/cm^2 at $T = 0°$C.

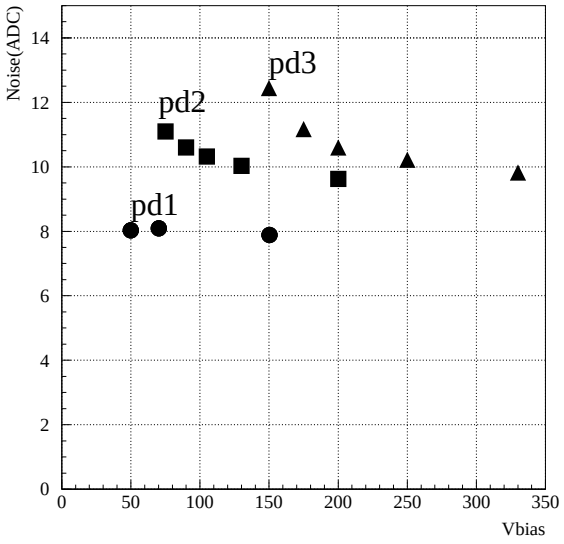

Figure 1: Noise vs $V_{\rm bias}$ for each detector.

[2)] The general noise formula $ENC = ENC_{\rm el} \bigoplus ENC_{\rm leak}$ becomes $ENC = (500 + 38 \cdot C_{\rm tot}[{\rm pF}]) \bigoplus (717\sqrt{I_{\rm leak/str}[\mu{\rm A}]})$ with the appropriate constants for the 128Premux. Taking the measured values for $C_{\rm tot} = C_{\rm inter} + C_{2^{\rm nd}{\rm neigh}} + C_{\rm bulk}$ (where $C_{2^{\rm nd}{\rm neigh}} \simeq 10\%$ of $C_{\rm inter}$ and $C_{\rm bulk} \simeq 0.16 * 11{\rm cm} = 1.8{\rm pF}$) and I_{leak} for each pair of detectors we have for the noise of each module: $ENC_{\rm pd1} = 901$, $ENC_{\rm pd2} = 1098$, $ENC_{\rm pd3} = 1132$.

[3)] Expecially considering that for CMS, using the whole readout chain with the APV6 readout chip instead of the 128PreMux, there is an additional noise factor of $\simeq 1.4$ in order to take into account the presence of the ADSP and of the analog optical link.

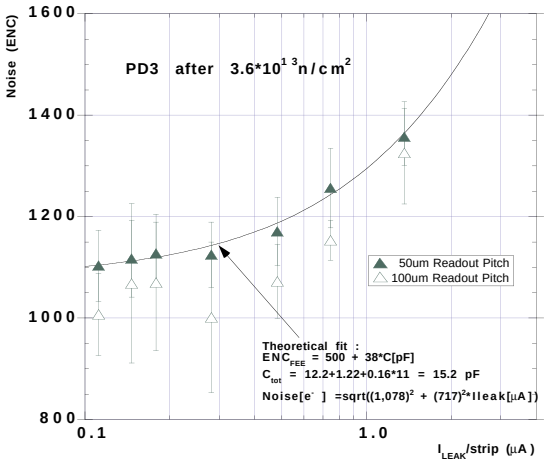

Figure 2: Noise comparison between 50 or 100 µm readout pitch vs. $I_{\rm leak}$ for *pd3*.

3 Test beam setup and data analysis

We tested our three modules with $120\ GeV$ pions at the X7 area at CERN, during 100 hours of SpS beam in September 1996.

The configuration we used for data taking is the same as described in [7] with our modules inserted one at a time in the middle (fig.3) of the 4 double-sided silicon planes offered by the *Bari telescope* [8]. This telescope allows for a tridimensional tracks reconstruction with a resolution in the vertical coordinate (the only one measured by our modules) $\leq$ 4.0 µm.

Data processing/analysis was performed using the TT5 package, developed at CERN by the Aleph/CMS collaboration, for both telescope planes and our detectors. This package allows for pedestal, single channel noise, common-mode noise, signal common-mode-subtracted and cluster selection to be calculated on an event by event basis using an algorithm described in [9]. This algorithm needs pre-determined thresholds, that we fixed to be the same for all our modules in order to have an exact performance comparison between them. Chosen thresholds are listed in the following table:

	$\perp$	20°	35°	telescope
(S/N) (central cut)	5	3	3	5
(S/N) (neighbor cut)	3	2.5	2.5	3
(S/N) (cluster cut)	6	6	6	10
Max ext. cluster	10	10	10	10
Max N deadstrip	3	3	3	3
Noise (upper thrs – ADC counts)	25	25	25	30
Noise (lower thrs – ADC counts)	5	5	5	2

Table 4: Values chosen for the constants used in our analysis with the TT5 package.

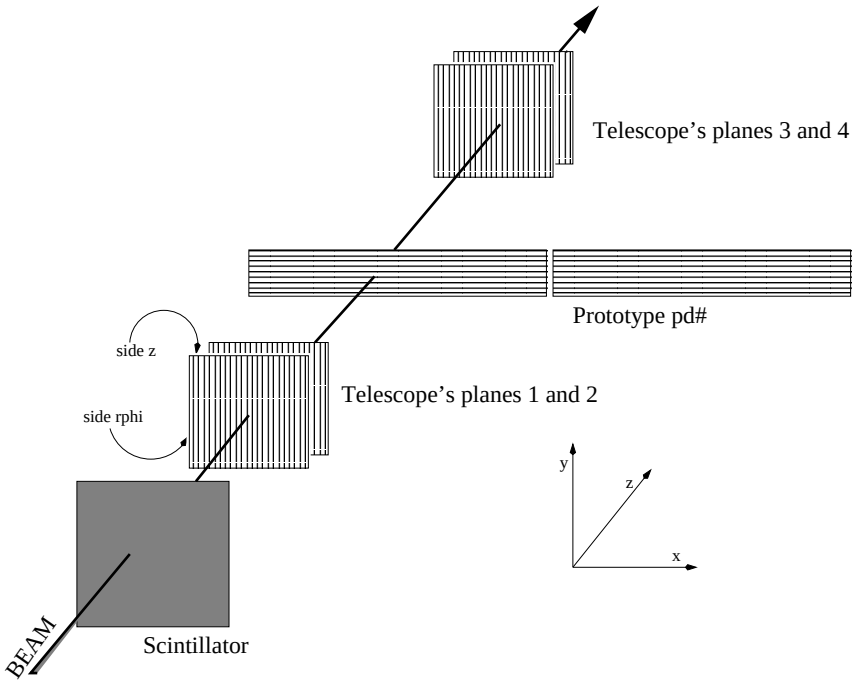

Figure 3: Test beam setup.

For our analysis we consider only the fraction of tracks with at least three points, both x and y, in the four telescope planes with the further requirements to be inside the geometrical acceptance of the detector under test. Finally tracks pointing in within one strip from "noisy" or "dead" channels in our detectors are also discarded.

4 Test beam results

We summarise our test beam results in three subsections. First we consider in detail charge collection and resolution as function of $V_{\rm bias}$ when tracks cross our detectors perpendicularly. Second, we analyse resolutions at large angles of incidence and finally we compare, for the most irradiated module, performances between 50 and 100 µm readout pitch.

4.1 Normal incidence

4.1.1 Signal/Noise ratio

Collected charge for *pd3* at 200 V is shown in fig.4. There is a well marked difference in the charge collected between 1-strip clusters and 2strips-clusters (fig.4). This is true for all detectors regardless of the dose and is due to a) delta rays, b) charge coupled to the adjacent strips, c) thresholds in clustering. For this reason we kept the different cluster size signals separated in fig.5.

In general we observe that:

1. irradiated detectors collect the same charge as the unirradiated one;

2. the collected signal grows with $V_{\rm bias}$ reaching an asymptotic value. If we define $V_{\rm working}$ as the working value for $V_{\rm bias}$ when the signal is 90% of its maximum, then $V_{\rm working} \simeq 1.5 \times V_{\rm depl}$ for all the devices.

Standing the previous results on the noise (fig.1), we compare in fig.6 the signal/noise for the three detectors as the ratio of the most probable value from the Landau fit (for all cluster sizes associated to a found track) with the average single strip noise. Values are plotted in "overdepletion scale" and compared with the signal/noise value of *pd1* unirradiated. The higher value for *pd1* is entirely due to its lower capacitance.

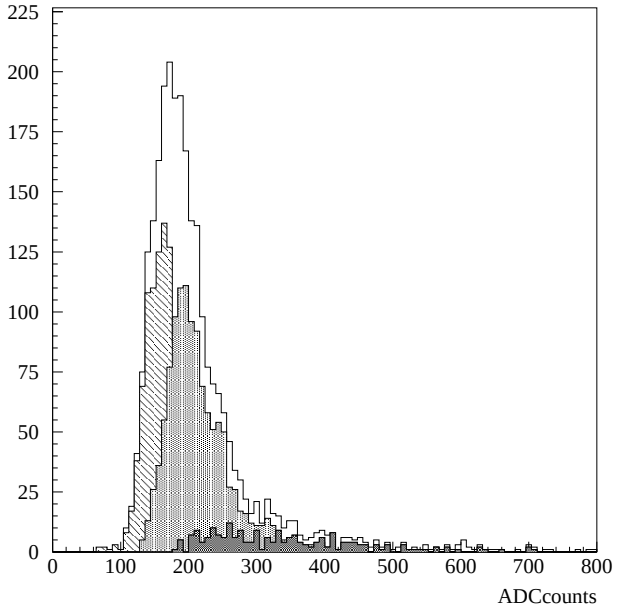

Figure 4: Charge collected for all cluster sizes (empty histo), 1-strip clusters (dashed), 2-strip clusters (filled) and 3-strip clusters (black) [from pd3@200V].

4.1.2 Cluster size

Fig.7 shows the cluster size distribution taken at $V_{\rm bias} = V_{\rm dep} \times 1.5$ for the three modules. There is an evident increase in the average cluster size for the irradiated detectors in spite of the increase in applied electric field. This can be understood in terms of an effective increase of the hole diffusion due to:

1. a lower value of mobility with irradiation favours diffusion with respect to drift motion.

2. after inversion, holes go through an electric field which is increasingly weaker in their motion toward the strip, again favouring diffusion.

3. a higher interstrip capacitance with a consequent higher capacitive coupling of the signal to the neighbour strips.

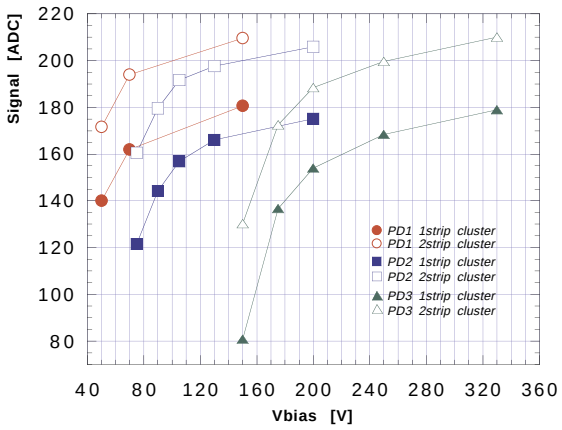

Figure 5: Signal collected at different $V_{\rm bias}$, according to cluster size.

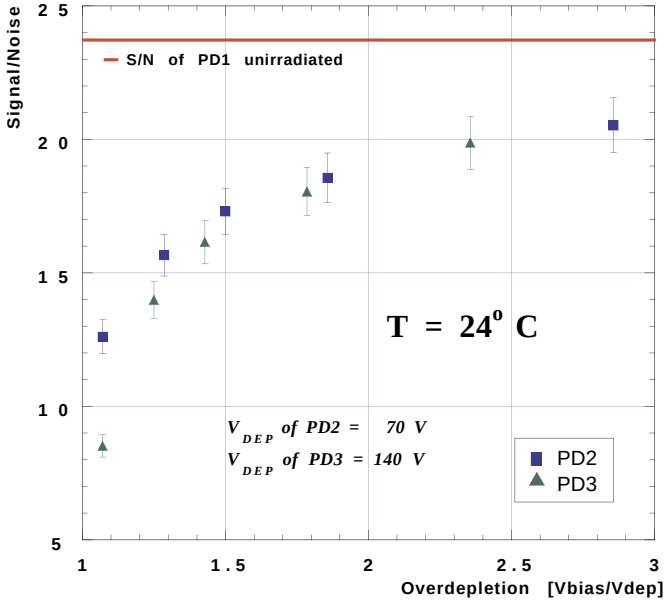

Figure 6: Signal/noise of the irradiated detectors compared to the value before irradiation. Abscissa is in overdepletion units, i.e. $V_{\rm bias}/V_{\rm depl}$. $V_{\rm depl}$ = 70 V for *pd2* and $V_{\rm depl}$ = 140 V for *pd3*

.

This increased diffusion may result in a better resolution of the detectors as long as the average track incidence angle is near the perpendicular, charge collection time is not critical and there is some signal/noise to spare.

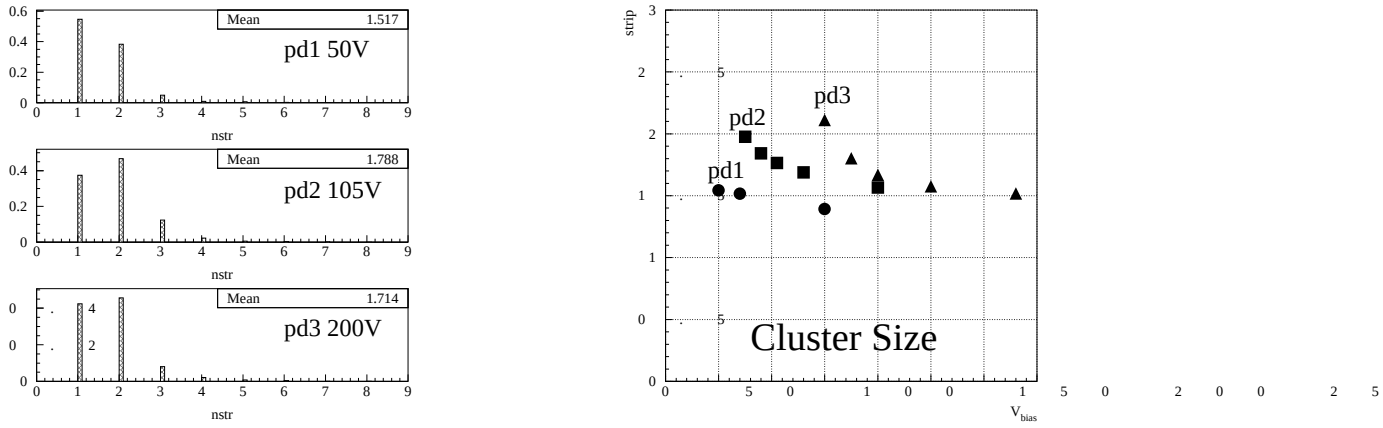

Figure 7: $V_{bias} \simeq 1.5 \times V_{depl}$), and mean cluster size values (at normal incidence) as a function of V_{bias}

.

4.1.3 Efficiency

Detectors efficiency is shown in fig.8. It is calculated as the ratio between the number of tracks predicted to cross the detector under test in within its geometrical acceptance (and away from "dead" or "noise" strips) and the number of tracks found. Except for low bias voltages this number is always above 99% as expected. Lost tracks are found randomly distributed inside the detectors and they correspond to fluctuations of the collected charge below the *seed strip* threshold cut.

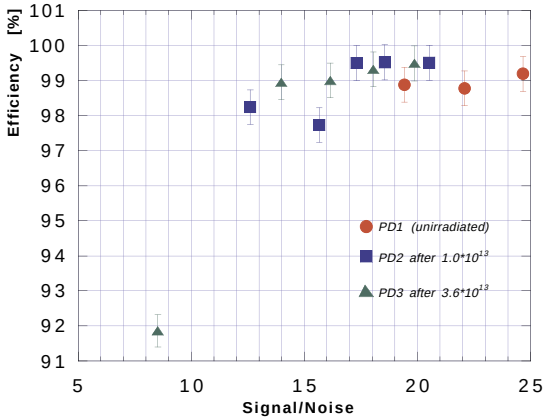

Figure 8: Detectors efficiency (at normal incidence) as a function of S/N ratio.

4.1.4 Spatial resolution

Since the two irradiated modules collect the same charge of *pd1* at a reasonable value of overdepletion and they also take advantage of a larger transversal diffusion, it is not surprising that they reach the same spatial resolution of *pd1* (fig.9). This is in spite of the fact that they have a lower signal/noise value. The concave shape of the curves for the three modules are easily understood considering that at low values of $V_{\rm bias}$ the detectors are not fully efficient in terms of charge collection and at high $V_{mathrmbias}$ the electric field is high enough to increase the ratio 1-strip clusters/2-strip clusters with the consequence of spoiling the resolution.

Plotted resolution values are calculated accordingly to the following:

1. 1-strip clusters resolution is defined as the RMS of the residuals distribution; residual is the distance between reconstructed track position and the center of the hit strip;

2. 3strip-cluster resolution is also the residuals RMS; in this case hit position is the cluster center of mass;

3. 2-strip clusters resolution is instead the standard deviation σ of the gaussian fit to the residuals distribution. To improve the resolution of this large fraction of clusters we applied a correction to the simple center of mass algorithm, in order to take into account the well-known "η" distortions. Details about this correction are explained in the next subsection.

4. finally the plotted resolution is taken as the weighted mean of 1-strip clusters, 2-strip clusters and 3-strip clusters resolutions subtracting in quadrature the telescope resolution (estimated to be $\simeq$ 4 µm)

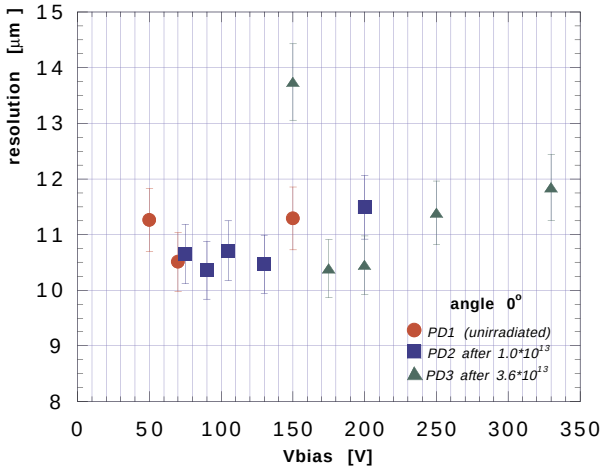

Figure 9: Detectors spatial resolution (at normal incidence).

4.1.5 Corrections to the center of mass algorithm

It is known that by simply using the center of mass algorithm, systematic errors are introduced in the reconstructed hit position. This is because the center of mass algorithm does not take into account a) the shape of the cloud of charge reaching the strip for collection and b) the strips capacitive coupling.

Evidence of these distortions can be easily seen in the interstrip distribution of the 2-strip clusters reconstructed position (fig.10). The center of mass method tends to accumulate the 2-strip cluster position toward the edges depleting the center between two strips (dashed histogram) where instead, as expected, most of the 2-strip cluster tracks have indeed crossed the detector in the middle between 2 strips (empty histogram).

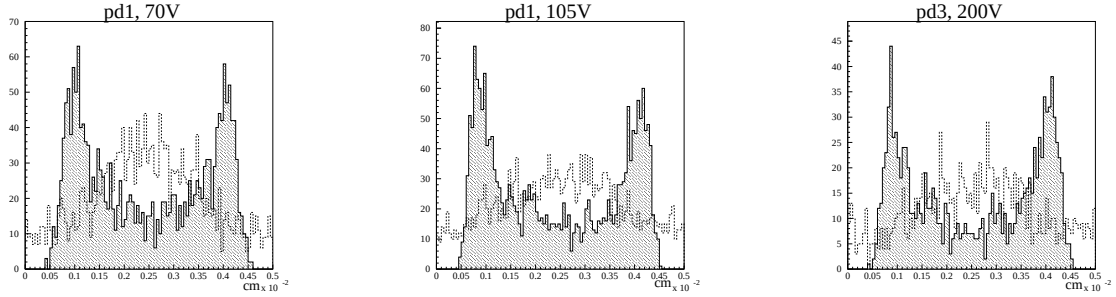

Figure 10: Position of cluster as determined by the center of mass algorithm (dashed), and the true track position determined by the tracking (empty) for the three detectors.

In principle one should be able, knowing exactly the charge diffusion during collection and the charge sharing between strips, to find the appropriate algorithm to correct for this distortion. In practice though, these parameters are far from being known with precision and therefore is easier to implement an *ad hoc* correction based on the difference between calculated and predicted position of the tracks (fig.11).

The correction (one set of parameters for each detector) simply flattens the distribution of fig.11 along the interstrip position and, applied to all runs taken, results in the improved residual RMS shown in fig.12.

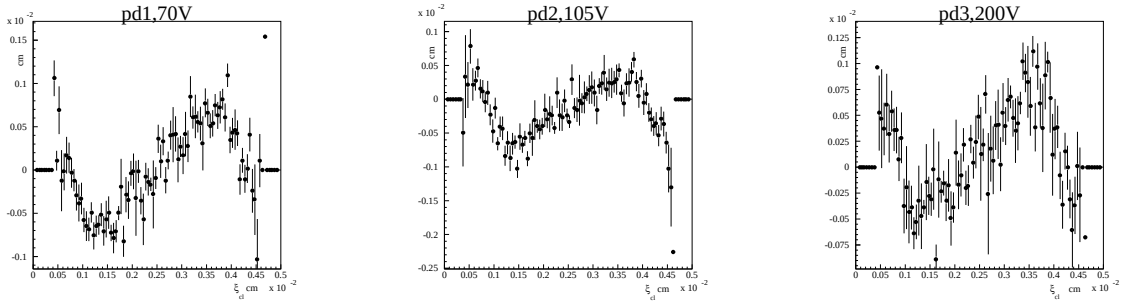

Figure 11: Residuals distribution of 2-strip clusters as a function of the interstrip position. The behaviour is the same for all detectors.

We also tried to better understand the combined effect of the shape of the collected charge cloud and the capacitive coupling to the neighbour strips using a one-dimensional simple model

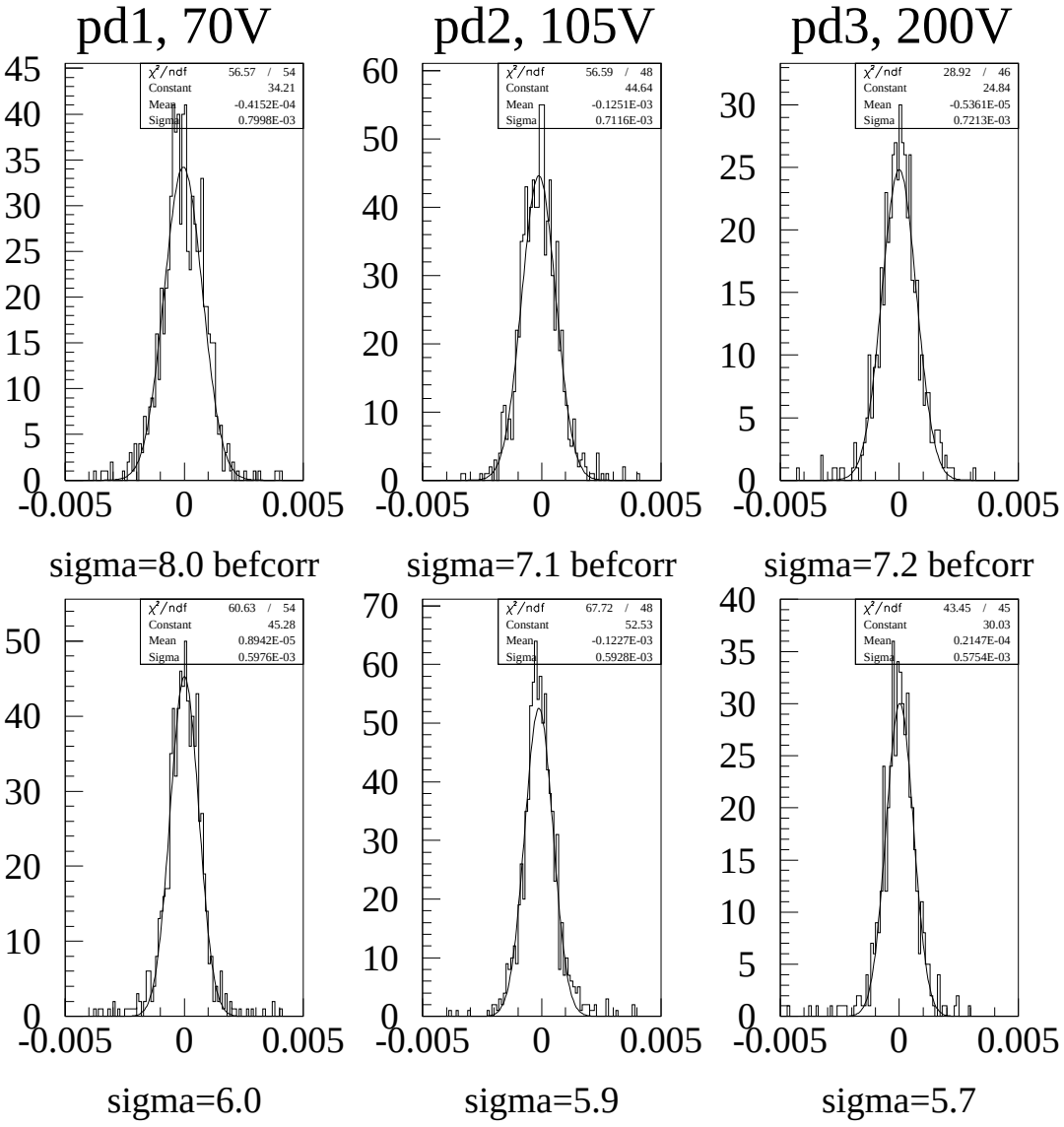

Figure 12: Residuals RMS for the three detectors before and after the applied correction. These distributions contain only 2-strip clusters.

with two free parameters. The model considers a) a gaussian shaped charge cloud (whose standard deviation is the first free parameter) and b) an identical fraction of charge spilled over the neighbor strips (this fraction is the second free parameter). In fig.13 is shown how this simple model fits very well the distributions shown earlier. But, even if the distribution shapes are well reproduced by this model, the values of the free parameters found are more of a problem. For instance the fit on *pd2* gives 6.6 µm for the σ of the gaussian distribution and 9.8% of spill over (both reasonable), but these values become 12 µm and 23% for *pd1*.

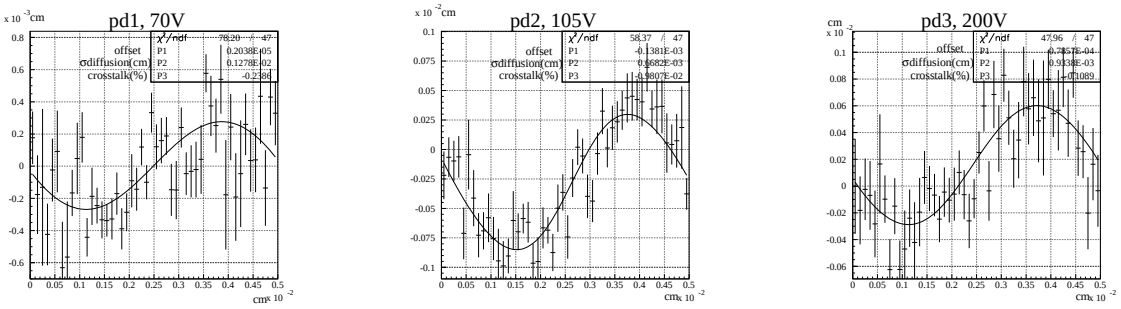

Figure 13: ame distribution as in fig.11 fitted with our 1-dim model for charge diffusion and charge capacitive coupling.

4.2 Large incidence angles

When particles cross the detector with an angle of 20° (or 35°) charge is shared typically among 3 (or 5) strips. In this case no benefits are expected from a larger transversal diffusion and differences in the detectors noise are relevant because less charge is collected by each single strip.

With incident angle equal to 20° we can consider only the charge collected into 3-strip clusters, largely the biggest fraction, while for the 35° case we consider both 4 and 5-strip clusters. The charge collected is shown in fig.14 and 15.

We observe that the collected charge is exactly the same before and after irradiation, as in the normal incidence case. Values from the different detectors are superimposed when plotted as function of overdepletion, i.e. $V_{\rm bias}/V_{\rm depl}$.

Plots in fig.16 and 17 are identical to fig.6, but in this case we chose to stress the difficulty posed by the multiple strips hit by plotting the "single-strip" **signal/noise** ratio (i.e. the total collected signal is divided by the number of strips in the cluster).

In these runs, the hit position is defined by the cluster center of mass without any correction. Consequently the resolution is the mean of the residuals RMS weighted on the different cluster size population. Resolutions are plotted in fig.18 and 19 as function of $V_{\rm bias}$.

With a 20° incidence there is little difference between the best value of *pd1*, $\sim$ 11 µm, and *pd2* and *pd3* values, $\sim$ 13 µm and $\sim$ 12 µm respectively. When instead the angle of incidence is 35° the difference becomes larger: *pd1* resolution is $\sim$ 19 µm while for *pd2* and *pd3* is around $\sim$ 23 µm.

This bigger difference with increased angle is entirely due to a more marginal signal/noise for the irradiated detectors and could have been partially recovered, as already noticed, by

appropriately lowering the threshold cuts for the clustering algorithm. In any case it seems clear that as long as the signal/noise can be kept above $\simeq$ 8 no significant resolution losses can be found while below this value it becomes rapidly very difficult to recover the original performances. This loss of resolution at large angles is the most noticeable difference found between irradiated and non irradiated detectors.

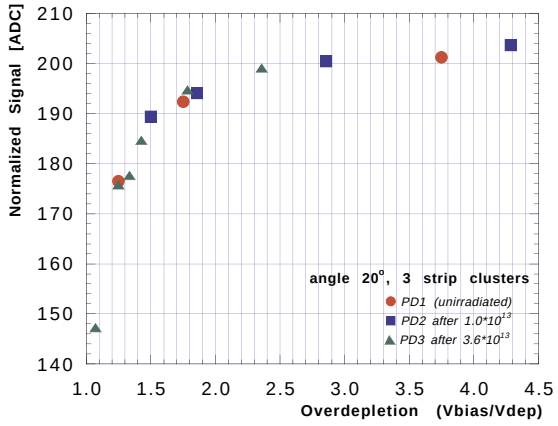

Figure 14: Most probable signal in 3-strip clusters with incidence 20°. The right axis is the normalised signal to be compared with signal collected at normal incidence.

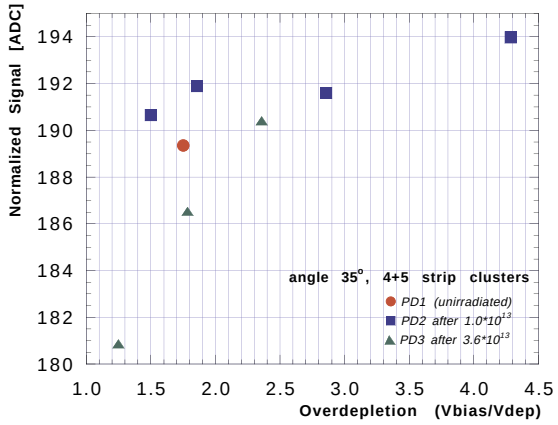

Figure 15: Same as 14 when angle of incidence is 35°, considering together 4- and 5-strip clusters.

4.3 50-100 μm readout pitch comparison

Toward the end of the data taking we decided to look at the difference in performance between 100 µm readout pitch (readout on every other strip) and the standard 50 µm readout pitch (readout on every strip). This was done only for *pd3* by disconnecting every other strip

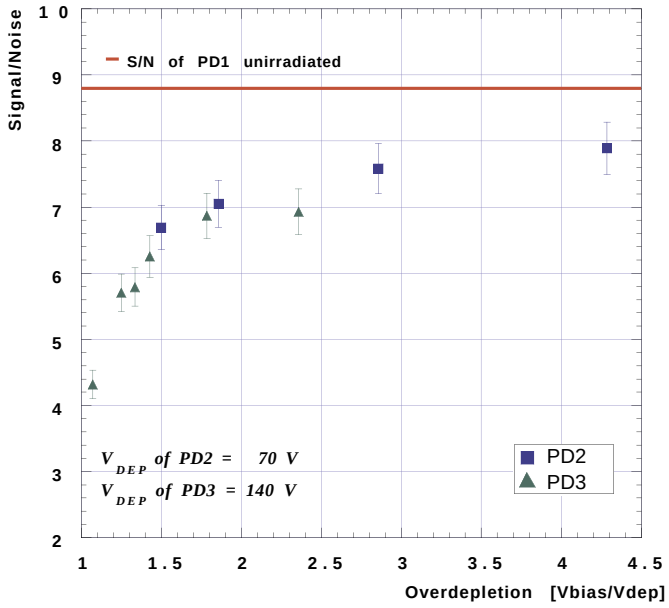

Figure 16: Most probable signal/noise ratio for a strip in a cluster in the irradiated devices compared with *pd1*, when tracks had an angle of 20°.

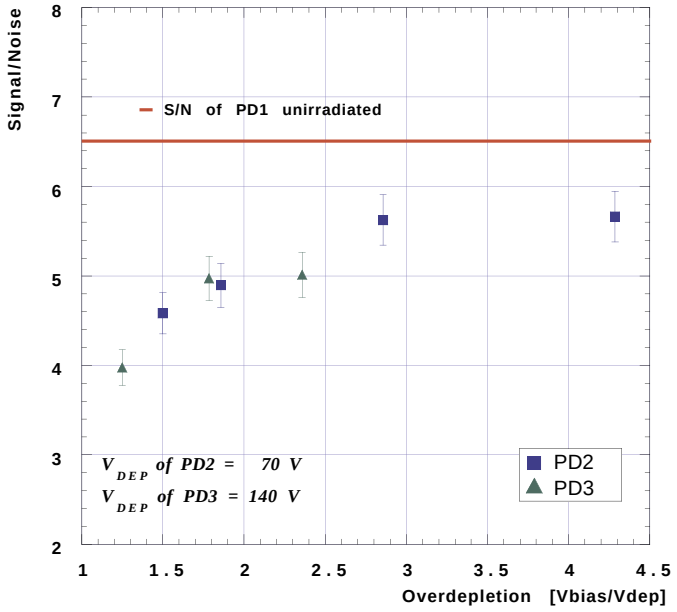

Figure 17: The same as 16 when the angle is 35°.

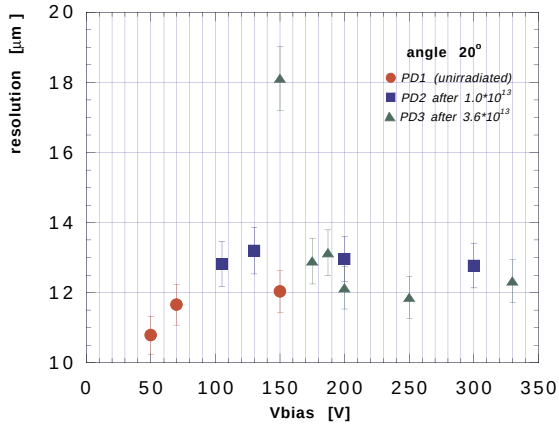

Figure 18: Spatial resolution for tracks with an incident angle of 20°.

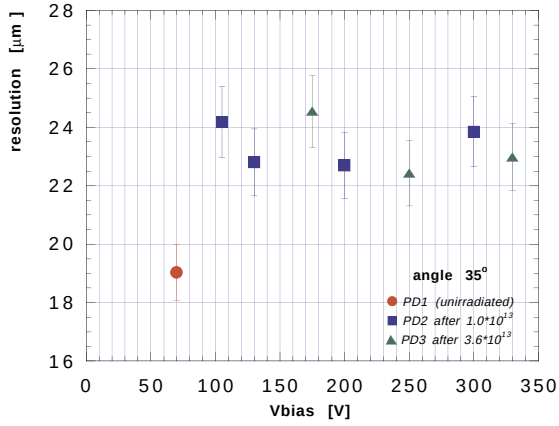

Figure 19: Spatial resolution for tracks with an incident angle of 35°.

from the readout chip on one half of the detector leaving the other half connected as before. This allowed us to compare under the same experimental conditions results on the two different readout pitches.

Unfortunately we had time only for a few runs, so we decided to concentrate our efforts at the highest applied bias voltage ($V_{\rm bias}$ = 330 V) and normal incidence angle.

We analysed these runs using the same parameters as in table 4 even though we know that there is margin for improvement by relaxing the demand on the signal/noise for the seed strip (parameter 1 on table 4).

For tracks passing near the floating strip the charge is collected by the neighbour strips with an efficiency that depends upon the value of the interstrip capacitance. This value is higher for the irradiated detectors and therefore we expect to have slightly better performances with respect to this phenomenon for the irradiated detectors. In fig.20 the total cluster **signal** is plotted as a function of the track position between two adjacent readout strips, both for 100 and 50 µm readout pitch. Only $\simeq$ 75% of the charge released in the silicon bulk is collected when the track goes near the floating strip and we found a value of 15.1 for the **signal/noise** (averaged over all cluster sizes and track positions) with the floating strip with respect to 19.9 without floating strip.

In fig.21 we show the tracks distribution for 2-strip clusters (left) and for single-strip clusters (right). As expected the 2-strip clusters distribution is widened by the floating strip (cfr. with fig.10). Fig.22 shows the residuals distribution for 1-strip clusters (RMS=16.3 µm) and 2-strip clusters (σ = 12.8 µm) when the readout is 100 µm. The weighted mean of these two values is 14.0 µm against 11.8 µm without floating strip. This results should be considered really good, considering that thresholds, clustering algorithm and $V_{\rm bias}$ were not optimised for this readout pitch.

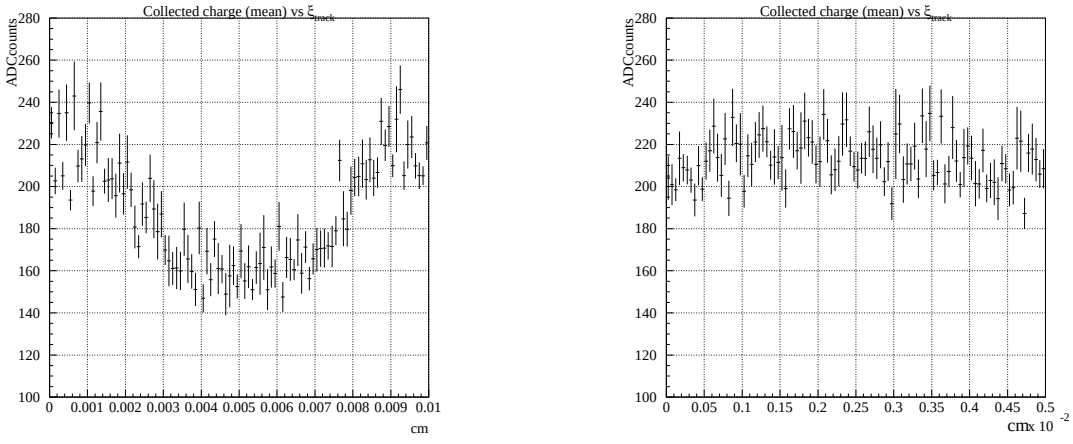

Figure 20: Charge collection as a function of interstrip position for 100 µm readout pitch (left) and for 50 µm readout pitch (rigth).

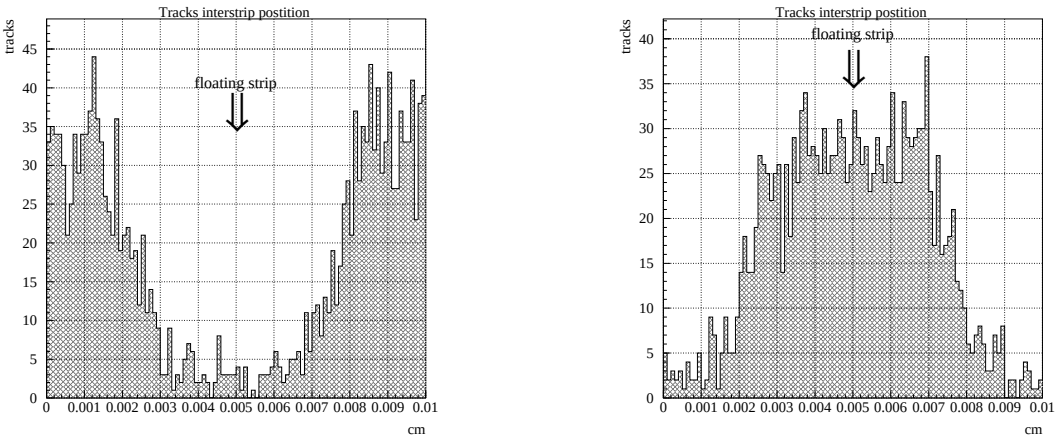

Figure 21: 1-strip cluster (left) and 2-strip cluster (right) interstrip distribution with 100 μm readout pitch.

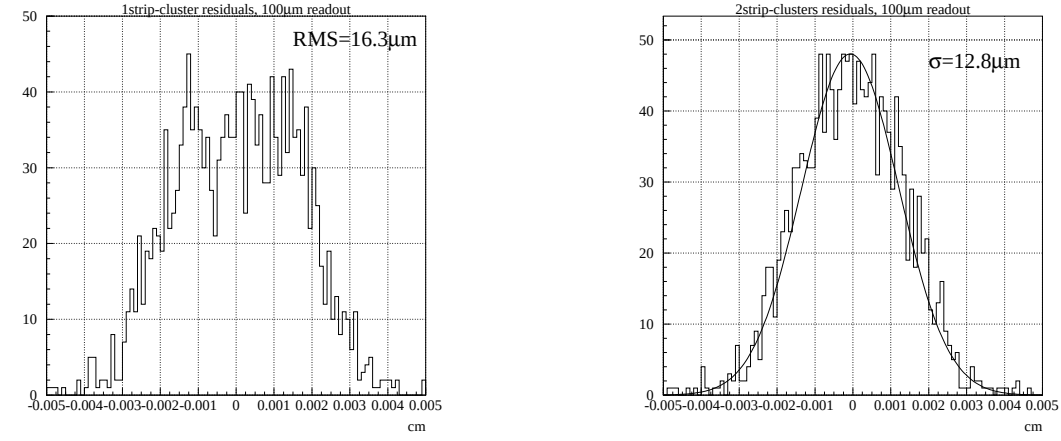

Figure 22: Residuals distribution with 100 μm readout pitch for 1-strip clusters (left) and 2-strip clusters (right). The weighted mean is 14 μm.

5 Conclusions

Single-sided silicon microstrip detectors can operate with almost identical performances up to radiation doses of several 10^{13} p/cm^2. The main performance loss due to radiation damage seems to be simply the increased interstrip capacitance which results in higher noise. Consequently, as long as the detectors can be operated at high enough (about $1.5 \times V_{\rm depl}$) bias voltages, their operation in a high dose environment is limited only by the leakage current increase. This increase should not dominate the overall noise value up to doses of $\simeq 2 \times 10^{14} {\rm p/cm}^2$ at 0°C which correspond to 10 years operation of LHC at a radius of 20 cm from the beam line.

References

[1] R.Wheadon et al., *RD20 Single-sided Prototypes (IC/SI)*, RD20/TN/20

[2] PSAIF; PS-ACOL neutron facility, CERN-HS-CFM/IR/91-10

[3] J.A.J.Matthews et al., *Bulk radiation damage in silicon detector and implication for LHC experiments*, NIM A 381 (1996) 338–348

[4] N.Bacchetta et al., *Radiation induced bulk damage in silicon diodes and implication for LHC experiments*, Proc. of the International Conference on radiation effects on semiconductor, Firenze (1996), NIM A 388 (1997) 318–322

[5] A.Peisert et al., *Evaluation of prototype detectors of the CMS tracker in a test beam*, CMS/TN/96-020

[6] L.Jones, *PreMux128 Specifications, version 2.1, December 19, 1994*

[7] O.Adriani et al., *Performance of a prototype of the CMS central Detector*, CMS/TN/95-118

[8] P.Tempesta et al., *A high resolution beam telescope built with double sided silicon detectors*, CERN-PPE/95-106

[9] P.Coyle et al., *Test beam results from prototypes of the upgraded Aleph vertex detector*, ALEPH 94-069